Bending Properties of Medium-Density Fiberboard and Plywood Obtained by Compression Bending Test

Hiroshi Yoshihara

Abstract

Compression bending testing, as described in this article, has been used successfully on various advanced composite materials, such as carbon-fiber reinforced plastics, to compute bending properties. This method might be applicable for several wood-based panels, such as medium-density fiberboard (MDF) and plywood, because they are quite thin, and thus the elastica phenomena can be easily induced. In this study, the bending properties of MDF and Lauan five-ply wood were determined by performing a compression bending test. The validity of the compression bending testing was then examined by comparing these results with the results from flexural vibration tests and three-point bending tests. The compression bending test proved effective for measuring the flexural Young's modulus when the length/thickness ratio was larger than 33 because the test method minimizes deflection caused by shearing force. Nevertheless, it was even less effective when the length/thickness ratio was smaller than 33. It was expected that the test would be more effective than the three-point bending test for measuring proportional limit stress and bending strength because the test specimen is independent of the stress concentration around the loading nose; however, this proved not to be the case for the materials investigated in this study. Thus, further research is still needed to devise ways to more effectively measure the bending properties of the materials tested.

Medium-density fiberboard (MDF) and plywood are common engineered wood products used in products where flexure is important. Reliable data on the bending properties of these materials are important to end users, such as manufacturers and design professionals.

In conventional bending tests such as three- and four-point bending tests, stress concentration at the loading point is significant (Whitney 1985, Hojo et al. 1987, Cui and Wisnom 1992). Therefore, there is a concern that bending properties, including Young's modulus, proportional limit stress, and bending strength, cannot be evaluated appropriately by the conventional bending tests. The stress concentration produces the excessive deflection, so the flexural Young's modulus is underestimated when using loading nose with a small radius (Yoshihara and Fukuda 1998). The stress concentration enhances the bending failure, so the bending strength is also underestimated when the radius of loading nose is small (Hojo et al. 1987). To address this potential concern, Fukuda (1989) developed a bending test for use on carbon-fiber–reinforced plastics. The test involves applying compression load along the long axis of a test specimen with a rectangular cross section and calculating the Young's modulus and bending strength from the observed elastica phenomena. This so-called compression bending test has been used on various advanced composite materials and solid wood (Fukuda 1993; Fukuda et al. 1995, 2002; Russell et al. 1998; Abry et al. 1999; Fukuda and Itabashi 1999; Shioya et al. 1999; Kallel-Kamoun et al. 2000; Mahieux and Reifsnider 2001; Yoshihara and Oka 2001), suggesting that this method is effective for the measurement of bending properties while reducing the influence of stress concentration.

MDF and plywood are more suitable than solid wood for measurement of bending properties by the compression bending test because they are quite thin, and thus the elastica phenomena can be easily induced. Nevertheless, there are as yet no examples of the test having been used on MDF and plywood. If the validity of the test can be verified for these materials, the test will find more frequent use.

In this study, we performed compression bending tests on MDF and plywood specimens to analyze the relationship between bending properties and specimen length. In addition, we performed three-point bending tests and used these test results to evaluate the validity of the compression bending test.

The author is Associate Professor, Faculty of Sci. and Engineering, Shimane Univ., Matsue, Shimane, Japan (yosihara@riko.shimane-u.ac.jp). This paper was received for publication in August 2010. Article no. 10-00031.

Forest Prod. J. 61(1):56–63.

Compression Bending Equation

Figure 1a shows the idealized model (free-body diagram) of the setup of the compression bending test. When axial load P is applied along the long axis of a rectangular beam of length L, the bending stress at the outer side of the midlength σ_{cb} is given by the equation (Timoshenko and Gere 1963)

$$\sigma_{cb} = \frac{6M}{BH^2} = \frac{6P\Delta}{BH^2} \tag{1}$$

where

B = beam width,

H = beam depth, and

Δ = deflection at the midlength.

Δ is obtained by measuring the loading-point displacement. If the loading-point displacement after the onset of flexure is X, the relationship between Δ/L and X/L is approximated by the equation (Yoshihara and Oka 2001)

$$\frac{\Delta}{L} = \begin{cases} 0.620\left(\dfrac{X}{L}\right)^{0.50} & \left(0 \le \dfrac{X}{L} \le 0.1\right) \\ 0.505\left(\dfrac{X}{L}\right)^{0.40} & \left(\dfrac{X}{L} > 0.1\right) \end{cases} \tag{2}$$

σ_{cb} is obtained by substituting P and Δ into Equation 2. For example, σ_{cb} = 25.8 MPa when L = 400 mm, X = 4 mm, B = 24 mm, H = 12 mm, and P = 600 N.

The longitudinal strain ε_{cb} at the extreme fiber in bending of the midlength is

$$\varepsilon_{cb} = \frac{H}{2\rho} \tag{3}$$

where

ρ = radius of curvature at the midlength.

The relationship between ρ/L and X/L is approximated by the equation (Yoshihara and Oka 2001)

$$\frac{\rho}{L} = \begin{cases} 0.157\left(\dfrac{X}{L}\right)^{-0.50} & \left(0 \le \dfrac{X}{L} \le 0.1\right) \\ 0.138\left(\dfrac{X}{L}\right)^{-0.56} & \left(\dfrac{X}{L} > 0.1\right) \end{cases} \tag{4}$$

ε_{cb} is obtained by substituting ρ obtained from Equation 4 into Equation 3. By measuring P and X, the σ_{cb} and ε_{cb} relationship can be determined so that the bending properties can be analyzed.

These formulations are based on beam theory, in which the shift of neutral axis and stress redistribution caused by the occurrence of material nonlinearity are not taken into account. Therefore, the bending properties are obtained in the quasi-elastic range.

Experiment

Materials

MDF and Lauan (*Shorea* sp.) plywood were investigated. The densities (±standard deviations) at 12 percent moisture content (MC) were 0.61 ± 0.01 and 0.51 ± 0.02 g/cm^3, respectively. The MDF and plywood panels were fabricated by Ueno Mokuzai Kogyo Co. (Himeji, Japan) and had the

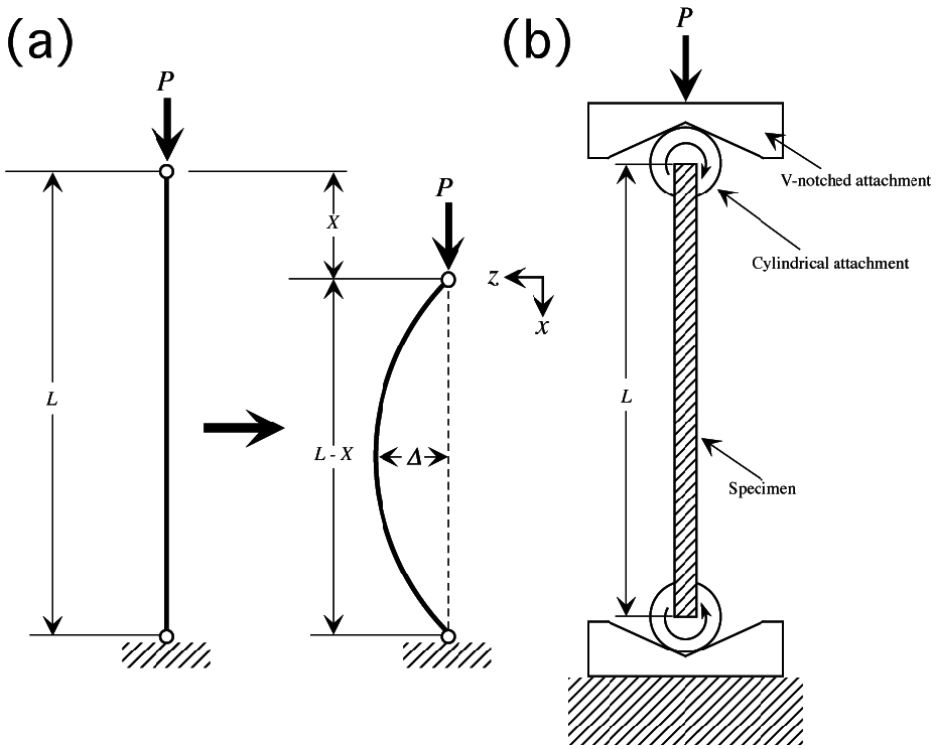

Figure 1.—(a) Idealized model (free-body diagram) with hinged ends bent under compression loading during the compression bending test; (b) test setup.

initial dimensions of 910 by 1,820 by 12 mm^3. The MDF was fabricated of softwood (typical fiber length 2 to 4 mm) and urea-formaldehyde resin. The plywood consisted of five veneers; the surface and core veneers (layers 1, 3, and 5) were approximately 1.8 mm thick, and the veneers adjacent to the surface veneer (layers 2 and 4) were approximately 3.3 mm thick. These materials were stored at a constant 20°C and 65 percent relative humidity before and during the test, and test specimens were confirmed to be in air-dried condition. These conditions were maintained throughout the tests. The equilibrium MC condition was approximately 12 percent. Seven specimens were tested under each test condition described below.

All test specimens were cut from the materials described above. Hereafter, the *x* axis is the length direction, the *y* axis is the width direction, and the *z* axis is the thickness direction of the sheet. Although MDF is usually regarded as an in-plane isotropic material, the fabrication process may induce alignment of the fibers, resulting in anisotropy (Kitahara 1963, Kazemi Najafi et al. 2007, Matsumoto and Nairn 2009). When a specimen is cut without consideration of directions, this anisotropy may prevent accurate measurement of bending properties. To address this concern, the length direction of the MDF specimen was made to coincide with the length direction of the sheet. For the plywood specimens, each was designated as either ''L-type'' or ''T-type,'' depending on whether the *x* axis of the surface and core veneers coincided with the longitudinal or tangential direction.

Compression Bending Tests

Figure 1b shows the setup for the compression bending test. Specimen dimensions were 250 to 500 (*x*) by 24 (*y*) by 12 (*z*) mm^3: specimen length *L* varied at intervals of 50 mm. The test apparatus contained a V-notched attachment and a cylindrical attachment with a Teflon sheet placed between them to enable the cylindrical attachment to rotate freely in the notch. Load *P* was applied at a crosshead speed of 1 mm/min until failures propagated significantly in the specimen. Loading-point displacement was determined from the observed crosshead displacement.

Figure 2a shows a typical plot of load versus loading-point displacement obtained for a compression bending test, and Figure 2b shows a sketch of the deformation and failure process under the compression bending loading. The illustration of catastrophic failure shows the typical bending failure. In the actual compression bending tests, however, various failure modes were observed. The details are described below. The curve reaches its peak value at the beginning of loading. The frictional force was not reduced entirely by the Teflon sheet. The specimen was therefore subjected to the fixed-end condition at the beginning of loading. When the specimen was compressed continuously, however, the cylindrical attachment rotated in the notch. The loading-point displacement at the peak of the curve is denoted Δu, and X can be set to either u or $(u - \Delta u)$.

Figure 3 shows typical stress–strain plots of σ_{cb} versus ε_{cb} obtained by setting X to either u or $(u - \Delta u)$. In the compression bending test, the value of compression stress σ_{cb} obtained by ignoring Δu first increases markedly, then peaks, and finally increases gradually until bending failure occurs. This behavior differs from that observed in a conventional bending test, in which bending failure usually occurs at the maximum bending stress. In contrast, the

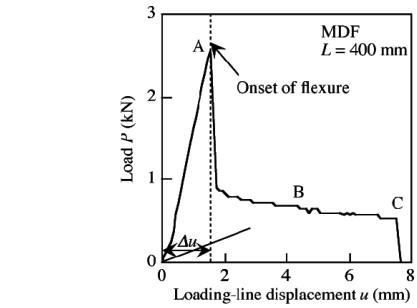

(a) Typical example of load/loading-line displacement relation

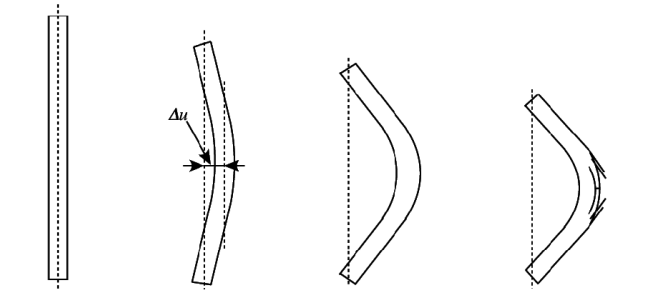

(b) Deformation and failure process

Figure 2.—Example of load versus loading-point displacement, measured by compression bending test; (b) sketch of the deformation and failure process.

stress–strain plot obtained by considering Δu is close to that observed in a conventional three-point bending test. Thus, the plot σ_{cb} versus ε_{cb} obtained by considering Δu is more valid than that obtained by ignoring it. Therefore, X was set to $(u - \Delta u)$ for the actual compression bending test. From the plot of σ_{cb} versus ε_{cb}, three bending properties were obtained: flexural Young's modulus E_{cb}, proportional limit stress Y_{cb}, and bending strength F_{cb}. A straight line was drawn from the origin, ignoring any initial deviations due to take-up of play in the loading on the plotted σ_{cb}–ε_{cb} curve

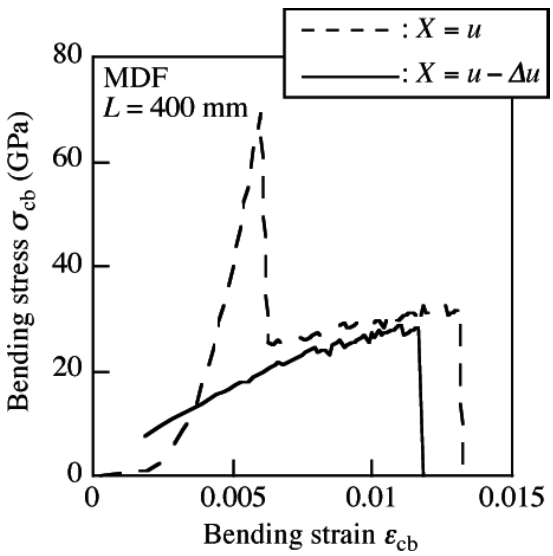

Figure 3.—Stress–strain plots obtained by setting X *to* u *and to* (u – Δu).

(Davies et al. 2001). E_{cb} was determined from the initial slope of the straight line. Y_{cb} was determined from the stress where the half thickness of the plotter trace deviated from the straight line (Davies et al. 2001). F_{cb} was determined from the stress at its maximum.

In the compression bending test, buckling behavior might influence stress–strain behavior after buckling, so buckling stress σ_b was determined and used for analysis of the stress–strain relationship in the postbuckling region. In the buckling test of a column, both the initial curvature of the specimen and any eccentricity in application of the load also influence buckling behavior. Therefore, we determined the critical load for buckling by Southwell's method, which takes these effects into account (Southwell 1932, Yoshihara 2010a). From the critical load P_c for buckling, the midlength deflection Δ is given with sufficient accuracy by

$$\Delta = \frac{a}{\frac{P_c}{P} - 1} \tag{5}$$

where

a = coefficient representing the influence of initial curvature and eccentricity in loading.

Accordingly, the relationship between Δ/P and Δ is

$$\frac{\Delta}{P} = \frac{1}{P_c} \cdot \Delta + \frac{a}{P_c} \tag{6}$$

Δ is calculated from the loading-point displacement X after the occurrence of buckling. The plot of Δ/P versus Δ was regressed into Equation 6 by the least-squares method, and P_c was calculated from the slope of the plot. σ_b was determined to be P_c/BH.

In addition to evaluating buckling stress by Southwell's method as just described, we also predicted it using Euler's elastic buckling equation and Engesser's tangent modulus equation (Timoshenko and Gere 1963). Euler's equation is

$$\sigma_b = \frac{\pi^2 E_{vib} H^2}{12L^2} \tag{7}$$

where E_{vib} is obtained by a vibration test, details of which are described below. However, this equation is not effective for columns of intermediate slenderness ratio. For Engesser's equation, the tangent modulus is usually defined as the local slope of a plot of stress versus strain obtained by compressing a short column (Timoshenko and Gere 1963, Yoshihara and Ohta 1995, Yoshihara et al. 1998). Nevertheless, it was difficult to obtain the stress–strain relationships of plywood and MDF properly because the materials are thin (Yoshihara 2010b). In this study, the tangent modulus was defined by E_{cb}, which can be regarded as the slope of a plot of stress versus strain at the occurrence of buckling, so Engesser's equation becomes

$$\sigma_b = \frac{\pi^2 E_{cb} H^2}{12L^2} \tag{8}$$

Flexural Vibration and Three-Point Bending Tests

Bending properties were evaluated by the flexural vibration and three-point bending tests. These properties were compared with the results from the compression bending test.A beam specimen with the dimensions of 500 (x) by 12 (y) by 12 (z) mm^3 was prepared. The Young's modulus in the length direction of the specimen E_{vib} was determined by a free-free flexural vibration test (Fig. 4). The specimen was suspended by threads at the nodal positions of the free-free resonance vibration mode f_n and excited in the x direction with a hammer. First- to fourth-mode resonance frequencies were measured and analyzed by a fast Fourier transform analysis program. E_{vib} was calculated by Hearmon's (1958) iteration method, which is based on an approximation of Timoshenko's flexural vibration solution that was developed by Goens (1931). In Hearmon's method, multiple resonance frequencies for flexural vibration modes are measured, and α and β corresponding to each mode are calculated as follows (Hearmon 1958):

$$\begin{cases} \alpha = \dfrac{4\pi^2 r L^2 f_n^2}{m_n^4}\left[-2m_n F(m_n) + m_n^2 F^2(m_n)\right] \\ \beta = \dfrac{4\pi^2 r A L^4 f_n^2}{m_n^4 I} \\ \qquad \times\left[1 + \dfrac{6m_n F(m_n) I}{L^2 A} + \dfrac{m_n^2 F^2(m_n) I}{L^2 A} - \dfrac{4\pi^2 r I f_n^2}{k G_{vib} A}\right] \end{cases} \tag{9}$$

where

G_{vib} = weak-axis shear modulus
r = density of the beam,
A = cross-sectional area,
I = secondary moment of cross-sectional area, and
k = shear correction factor, which is 5/6 that for a beam with a rectangular cross section.

The coefficients m_n and $F(m_n)$ that correspond to the resonance mode are

$$\begin{cases} m_1 = 4.730 \\ m_2 = 7.853 \\ m_n = \dfrac{(2n+1)\pi}{2} \qquad (n \geq 3) \end{cases} \tag{10}$$

and

$$\begin{cases} F(m_1) = 0.9825 \\ F(m_2) = 1.0008 \\ F(m_n) = 1 \qquad (n \geq 3) \end{cases} \tag{11}$$

The plot of α versus β for each mode was regressed into the linear function $\beta = q - p\alpha$, and E_{vib} and G_{vib} were to be q and q/kp, respectively. Initially, a virtual value of G_{vib} was substituted into β of Equation 5, and the refined value of

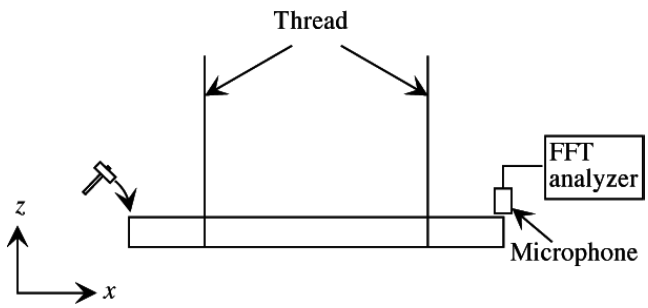

Figure 4.—Flexural vibration test for determining Young's modulus E_{vib}.

G_{vib} as q/kp was substituted into β again, and the procedure was repeated to give the regressed values of E_{vib} and G_{vib}. The value of E_x obtained by this method is free from the influence of deflection caused by shearing, so it is desirable that the Young's modulus obtained by the compression bending test is close to the E_{vib} value.

After conducting the flexural vibration test, the bending properties were measured using a three-point bending test. The specimen was supported by the 432-mm spans, so the span/depth ratio was 36. The span/depth ratio varies according to several standards. In BS EN 310 (British Standards Institution 1993), the span/depth ratio is determined as 20. In ASTM D1037 (American Society for Testing and Materials [ASTM] 2005), the span/depth ratio is determined as 24. In ASTM D3043 (ASTM 2003), the span/depth ratio is determined as 48 and 24 for the L-type and T-type plywood specimens, respectively. To measure the flexural Young's modulus precisely, the span/depth ratio is preferable to be large. Because of the limitation of testing apparatus, however, the span/depth ratio of 36 was utilized for every specimen in this study. In addition, the specimen width was 24 mm, which was similar to that of the compression bending test, although it is determined as 50 mm in the standards described above. Load P was applied to the midspan at a crosshead speed of 1 mm/min until the specimen failed. The deflection Δ at the bottom of the center was measured by a linear-displacement gauge set below the specimen. A straight line was drawn from the origin, ignoring any initial deviations due to take-up of play in the loading on the plotted P–Δ curve (Davies et al. 2001). The bending Young's modulus E_{tpb} was calculated by substituting the initial slope of the straight line into the following equation:

$$E_{tpb} = \frac{l^3}{4BH^3}\frac{\Delta P}{\Delta \delta} \tag{12}$$

where

l = span length.

The proportional limit stress Y_{tpb} and bending strength F_{tpb} were obtained from the following equations:

$$Y_{tpb} = \frac{3P_y l}{2BH^2} \tag{13}$$

and

$$F_{tpb} = \frac{3P_f l}{2BH^2} \tag{14}$$

where

P_y = load at the proportional limit and

P_f = maximum load.

The value of P_y was determined from the stress where the half thickness of the plotter trace deviated from the straight line (Davies et al. 2001).

Results and Discussion

In the compression bending test, the specimen was braced at the mid-length and any lateral torsional buckling was not observed.

Figure 5 shows plots of Young's moduli E_{cb}, E_{vib}, and E_{tpb} versus the length of specimen L. The statistical analysis of the difference between the E_{cb} and E_{vib} revealed that the difference is not significant when L is ≥400 mm, whereas E_{tpb} is significantly smaller than E_{cb} and E_{vib} at the significance level of 0.01. This result suggests that the compression bending test is available for measuring the flexural Young's modulus with reducing the influence of shearing force when L is ≥400 mm. When L is <400 mm, however, E_{cb} is significantly smaller than E_{vib} and E_{tpb} at the significance level of 0.01, so the flexural Young's modulus is not measured properly. Figure 6 shows plots of the buckling stress σ_b versus L, obtained by Southwell's method and predicted by Euler's and Engesser's equations. When L is ≥400 mm, σ_b obtained by Southwell's method and Engesser's tangent modulus are close to that predicted by Euler's equation. For small L, however, σ_b obtained by Southwell's method is smaller than that predicted by Euler's equation. In contrast, Engesser's tangent modulus theory is effective in predicting buckling stress, although E is provisionally used as the tangent modulus. This result suggests that the reduced stiffness induced by the axial load as well as the buckling stress dominates the stress–strain relationship in the postbuckling region. Because of this phenomenon, compression bending test is not effective for

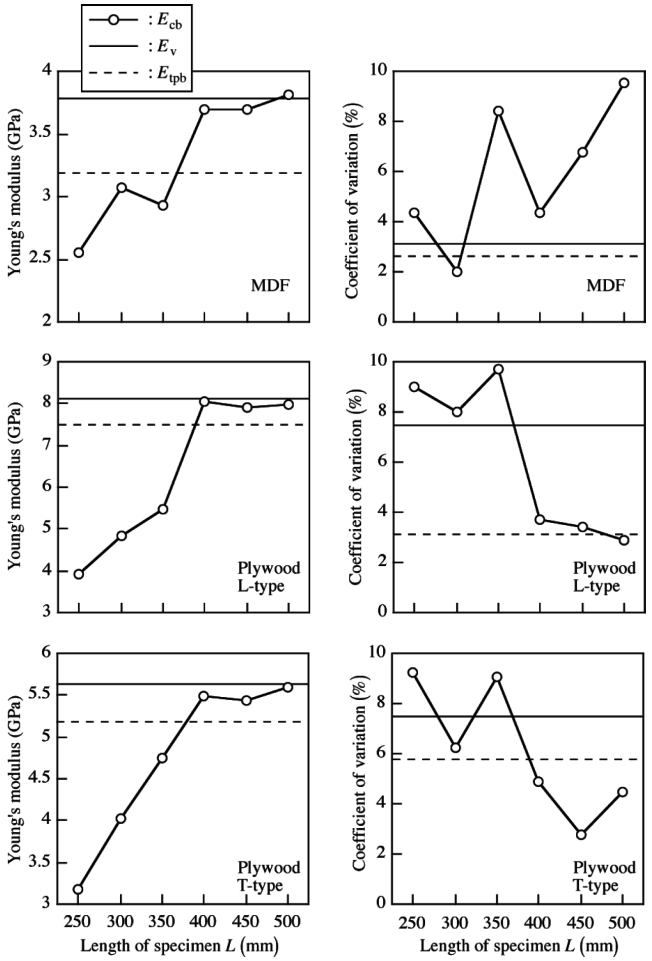

Figure 5.—Young's modulus versus specimen length, measured by the compression bending test and the three-point bending test. E_{cb} E_{vib}, *and* E_{tpb} *were obtained from the compression bending, flexural vibration, and three-point bending tests, respectively.*

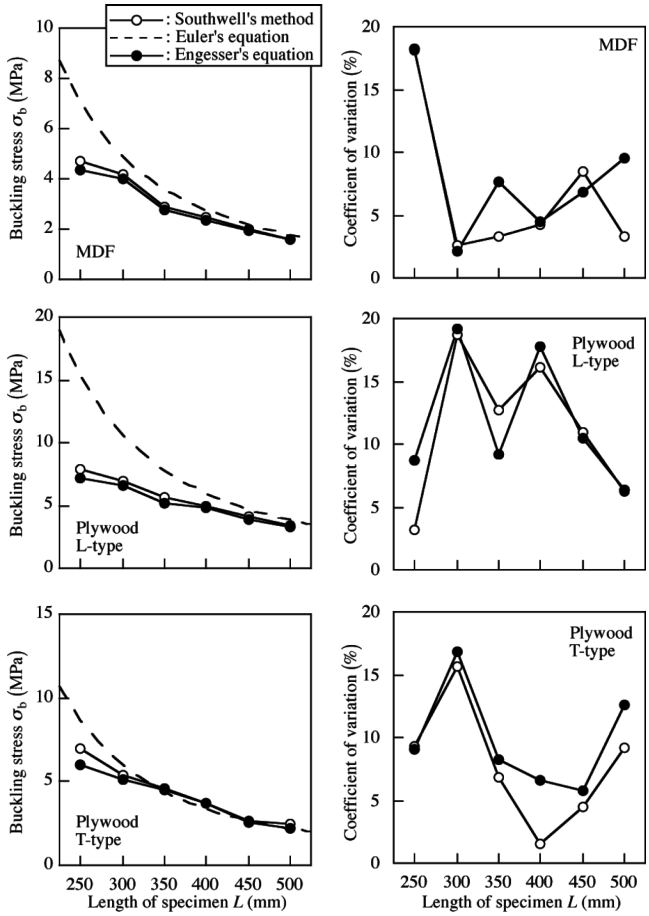

Figure 6.—Buckling stress versus specimen length, obtained by Southwell's method and predicted by Engesser's and Euler's equations.

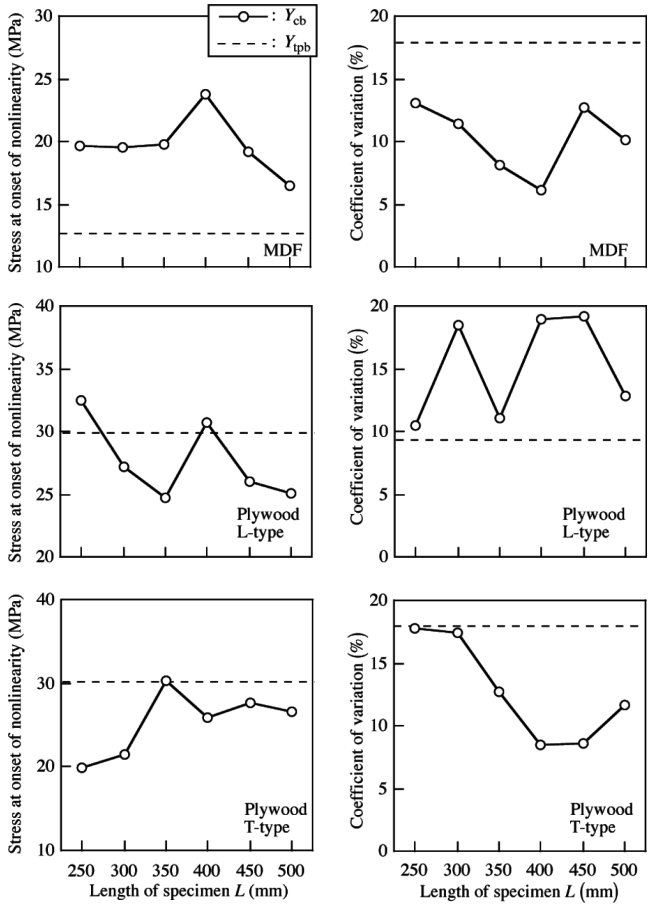

Figure 7.—Proportional limit stress versus specimen length, measured by the compression bending test and the three-point bending test. Y_{cb} *and* Y_{tpb} *were obtained from the compression bending and three-point bending tests, respectively.*

measuring the flexural Young's modulus when L is <400 mm.

Figure 7 shows plots of the proportional limit stresses Y_{cb} and Y_{tpb} versus L. The statistical analysis suggested that in MDF, Y_{cb} is significantly larger than the Y_{tpb} at the significance level of 0.01. In contrast, it also suggests that the influence of the test method on the values is not significant in plywood specimens.

Figure 8 shows plots of the bending strengths F_{cb} and F_{tpb} versus L. The statistical analysis suggested that in all materials, the F_{cb} is always smaller than the F_{tpb} at the significance level of 0.01.

Figure 9 shows the typical failure patterns of the specimens obtained by the compression bending tests. In the three-point bending test, bending failure is usually induced at the midlength of the tension side of the specimen when the load is close to its peak. In the MDF specimens, however, the failure often initiated at the peak load, and it propagated from the compression side without inducing the failure at the tension side (top of Fig. 9). In the T-type plywood specimens, however, the failure was often induced at the core veneer close to the loading point by rolling shear mode, and it gradually propagated along the neutral axis (core veneer) during increasing the bending stress (bottom of Fig. 9). These failures precede the bending failure at the tension side of the midlength. Therefore, the small value of F_{cb} may be because of these failure modes, so the F_{cb} values obtained from the MDF and T-type plywood specimens cannot be evaluated as the actual bending strength of the material. This issue indicates the superiority of the conventional bending method to the compression bending method for the MDF and T-type plywood specimens. For the L-type plywood specimens, however, the bending failure was induced at the midlength (middle of Fig. 9), similar to the results of the three-point bending tests. Further research should be conducted to reveal the reason for the small value of F_{cb}. In addition, these failures may induce the shift of neutral axis, which has a significant influence on the load–deflection relationship, and the shift of neutral axis might influence on the value of E_{cb} when $L < 400$ mm. Further research is also required to reveal the relationship between the failure modes and load–deflection behaviors, although the shift of neutral axis was not taken into account in this study.

As described in the introduction, the compression bending test can be performed without using the loading nose, so Y_{cb} and F_{cb} values are expected to be larger than Y_{tpb} and F_{tpb} values. Nevertheless, except for the values of Y_{cb} in MDF, satisfactory results were not obtained. The stress–strain relationship obtained from Equations 1 and 3 was derived based on simple beam theory without considering the shearing force. In addition, any stiffness distribution in the thickness direction, intrinsic to MDF and

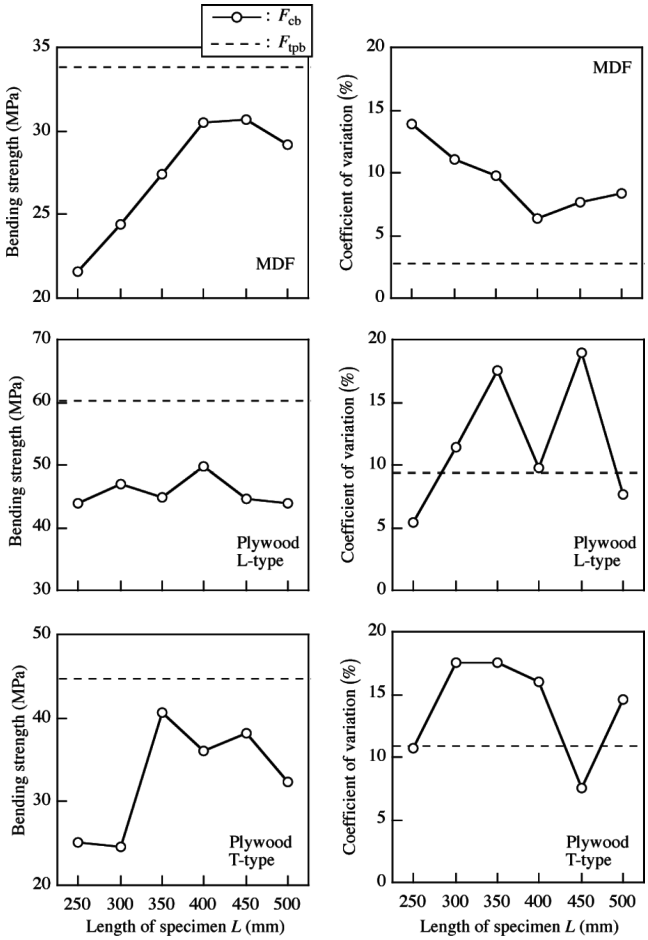

Figure 8.—Bending strength versus specimen length, measured by the compression bending test and the three-point bending test. F_{cb} and F_{tpb} were obtained from the compression bending and three-point bending tests, respectively.

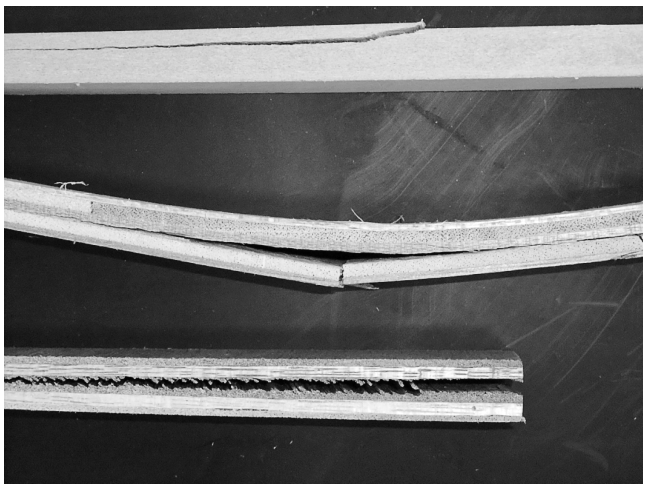

Figure 9.—Typical failure patterns of the specimens obtained by the compression bending test. From top to bottom: medium-density fiberboard, L-type specimen of plywood, and T-type specimen of plywood.

plywood, was also neglected in the stress–strain relationship. In the actual compression bending test, however, the stress distribution in the specimen is complicated by the shearing force and stiffness distribution, so the stress–strain relationship obtained from Equations 1 and 3 should be refined. In addition, the length/thickness ratio investigated in this study was smaller than 42. If the ratio is larger than 42, better results may be obtained. From these points of views, further research is still needed to devise ways to more effectively measure the bending properties of the materials tested.

Conclusions

The compression bending test was performed for MDF and plywood with the thickness of 12 mm. The validity of the test was then examined by comparing these results with those from the flexural vibration and three-point bending tests.

The compression bending test proved effective for measuring flexural Young's modulus because the test method minimizes deflection caused by shearing force when the length of specimen L was larger than 400 mm. Nevertheless, it was even less effective when L was smaller than 400 mm. It was expected that the test would be more effective than the three-point bending test for measuring proportional limit stress and bending strength because the test specimen is independent of the stress concentration around the loading nose; however, this proved not to be the case for the materials investigated in this study. Thus further research is still needed to devise ways to more effectively measure the bending properties of the materials tested.

Literature Cited

Abry, J. C., S. Bochard, A. Chateauminois, M. Salvia, and G. Giraud. 1999. In situ detection of damage in CFRP laminates by electrical resistance measurements. *Compos. Sci. Technol*. 59:925–935.

American Society for Testing and Materials (ASTM). 2003. Standard test methods for structural panels in flexure. ASTM D3043-00. ASTM, West Conshohocken, Pennsylvania.

American Society for Testing and Materials (ASTM). 2005. Standard test methods for evaluating properties of wood-based fiber and particle panel materials. ASTM D1037-99. ASTM, West Conshohocken, Pennsylvania.

British Standards Institution (BSI). 1993. Wood-based panels. Determination of modulus of elasticity in bending and of bending strength. BS EN 310:1993. BSI, London.

Cui, W. C. and M. R. Wisnom. 1992. Contact finite element analysis of three- and four-point short-beam bending of unidirectional composites. *Compos. Sci. Technol*. 45:323–334.

Davies, P., B. R. K. Blackman, and A. J. Brunner. 2001. Mode II delamination. *In:* Fracture Mechanics Testing Methods for Polymers Adhesives and Composites. D. R. Moore, A. Pavan, and J. G. Williams (Eds.). ESIS Publication 28. Elsevier, Amsterdam. 298 pp.

Fukuda, H. 1989. A new bending test method of advanced composites. *Exp. Mech*. 29:330–335.

Fukuda, H. 1993. Compression bending test method for advanced composites. *J. Jpn. Soc. Aero. Sci*. 41:482–487.

Fukuda, H. and M. Itabashi. 1999. Simplified compression bending test method for advanced composites. *Composites A* 30:249–256.

Fukuda, H., H. Katoh, and H. Uesugi. 1995. A modified procedure to measure bending strength and modulus of advanced composites by means of compression bending. *J. Compos. Mater*. 29:195–207.

Fukuda, H., T. Watanabe, M. Itabashi, and A. Wada. 2002. Compression bending test for CFRP pipe. *Compos. Sci. Technol*. 62:2075–2081.

Goens, E. 1931. Über die Bestimmung des Elastizitätsmodulus von Stäben mit Hilfe von Biegungsschwingungen. *Ann. Physik Ser. 7* 11: 649–678.

Hearmon, R. F. S. 1958. The influence of shear and rotatory inertia on the free flexural vibration of wooden beams. *Brit. J. Appl. Phys*. 9: 381–388.

Hojo, M., Y. Noguchi, H. Furue, and J. Matsui. 1987. Test method for flexural properties of unidirectional laminates reinforced with 4 GPa-class carbon fibers. *Reinforced Plast*. 33:2–11.

Kallel-Kamoun, I., A. Chateauminois, and F. Sidoroff. 2000. Secondary effects in the analysis of the post-buckling bending test. *Compos. Struct*. 50:85–92.

Kazemi Najafi, S., A. Abbasi Marasht, and G. Ebrahimi. 2007. Prediction of ultrasonic wave velocity in particleboard and fiberboard. *J. Mater. Sci*. 42:789–793.

Kitahara, K. 1963. On the anisotropy of fiberboard and particleboard. *J. Mater. Res. Soc. Jpn*. 12:722–726.

Mahieux, C. A. and K. L. Reifsnider. 2001. Property modeling across transition temperatures in PMC's: Part II. Stress rupture in end-loaded bending. *Appl. Compos. Mater*. 8:235–248.

Matsumoto, N. and J. A. Nairn. 2009. The fracture toughness of medium density fiberboard (MDF) including the effects of fiber bridging and crack-plane interference. *Eng. Fract. Mech*. 76:2748–2757.

Russell, B. E., C. A. Mahieux, and K. L. Reifsnider. 1998. Stress rupture of PMC's in end-loaded bending. *Appl. Compos. Mater*. 5:151–159.

Shioya, M., M. Nakatani, and K. Nakao. 1999. Axial compression bending tests on carbon films and carbon fiber composites. *J. Mater. Sci*. 34:1301–1311.

Southwell, R. V. 1932. On the analysis of experimental observations in problems of elastic instability. *Proc. R. Soc. Lond. A* 135:601–616.

Timoshenko, S. P. and J. M. Gere. 1963. Theory of Elastic Stability International Edition. McGraw-Hill, Singapore. 49 pp.

Whitney, J. M. 1985. Elasticity analysis of orthotropic beams under concentrated loads. *Compos. Sci. Technol*. 22:167–184

Yoshihara, H. 2010a. Analysis of the elastic buckling of a plywood column. *Mater. Struct*. 43:1075–1083.

Yoshihara, H. 2010b. Characterization of the in-plane compressive properties of plywood by IITRI and end-loading compression tests. *Wood Fiber Sci*. 42:409–411.

Yoshihara, H. and A. Fukuda. 1998. Influence of loading nose in the static bending test of wood. *J. Wood Sci*. 44:473–481.

Yoshihara, H., Y. Kubojima, and M. Ohta. 1998. Prediction of the buckling stress of intermediate wooden columns using the secant modulus. *J. Wood Sci*. 44:69–72.

Yoshihara, H. and M. Ohta. 1995. Analysis of the buckling stress of an intermediate wooden column by the tangent modulus theory. *Mokuzai Gakkaishi* 41:367–372.

Yoshihara, H. and S. Oka. 2001. Measurement of bending properties of wood by compression bending tests. *J. Wood Sci*. 47:262–268.